Combustion and Flame 180 (2017) 175–183

Contents lists available at ScienceDirect

Combustion and Flame

journal homepage: www.elsevier.com/locate/combustflame

Assembly and encapsulation of aluminum NP's within AP/NC matrix and their reactive properties

Haiyang Wang, Rohit J. Jacob, Jeffery B. DeLisio, Michael R. Zachariah*

Department of Chemical and Biomolecular Engineering and Department of Chemistry and Biochemistry, University of Maryland, College Park, MD 20742, United States

ARTICLE INFO

Article history:
Received 3 November 2016
Revised 3 January 2017
Accepted 28 February 2017
Available online 24 March 2017

ABSTRACT

Aluminum nanoparticles (Al NPs) are commonly employed as fuel supplement to increase the energy density of propellants. However, due to the highly agglomerated state of the NPs and significant pre-combustion sintering, ignition and combustion are not as facile as they could be. In this work, we employed a spray approach to generate near monodisperse microparticles of Al NP's encapsulated within ammonium perchlorate (AP) and a binder (nitrocellulose (NC)) The results show that Al/AP/NC composites have an ignition temperature (~700 K), which is significantly lower than Al melting point (~933 K). The reactivity of Al/AP/NC composites was also tested in a confined cell where we find that although the peak pressure for Al/AP/NC is comparable to that of physically mixed Al/CuO nanothermite, the impulse generated is more than two times higher. The measured flame temperature of Al/AP/NC composites were as high as 2800 K, which is ~500 K higher than Al/AP composites without NC. Furthermore, the potential mechanism for the early ignition of these composites were investigated. It is proposed that gaseous acid released from AP could play an important role in weakening the protective oxide shell on Al nanoparticles which could subsequently lead to the reaction of Al in the high-pressure oxygenated environment at lower temperature.

1. Introduction

Composite propellants common in solid-fuel rockets are primarily constituted of metal fuels, oxidizer crystals, and binder [1]. Conventionally, micron aluminum powders (3–20 μm) are employed as fuel due to their high enthalpy and ease of availability as an energy additive [2–4]. The aluminum particles are surface passivated by the naturally occurring oxide shell, which raises the ignition temperature of these particles to 2000–2300 K [5–7]. Typically aluminized composite propellant surface burning temperature is ~800 K [8,9], which leads to the ignition of micron Al to occur after a delay and away from the propellant burning surface, resulting in little heat feedback to drive flame propagation. Consequently, the addition of micron Al does not significantly result in enhanced burn rates. The replacement of micron Al with aluminum nanoparticles (Al NPs) markedly reduces the ignition delay and ignition temperature (<1000 K) [10,11], which leads to the aluminum particles burning closer to the propellant surface. This produces continuous heat feedback, resulting in a burn rate increase of as much as 100% [12,13]. However, Al NPs suffer from significant processing challenges due to their high specific surface area [4,14,15], which greatly increases the viscosity of the polymer binder matrix, limiting the nanometallic fuel content in propellants. Moreover, the pre-combustion coalescence of Al NPs increases their effective size to the micron scale, retarding ignition [14]. Last but not least, because of the high evaporation temperature of Al (~2700 K) [16], it exists as a condensed liquid droplet for long periods of time resulting in the formation of larger droplets prior to ignition. All of these factors minimize the potential applications as accelerating agents in propellants.

In our previous studies, small amounts of nitrocellulose (NC) were used to assemble Al NPs into uniform Al/NC microparticles, which not only decreases the processing difficulty, but also highly reduces the ignition delay time of Al NPs, resulting in a ~35% increase in propellant burn rates [17,18]. Significant efforts in the past, directed at tuning the burning rate of propellants involved adjusting the size of AP [19,20], using novel oxidizers in propellants [21], using catalyzing agents such as reactive wires [22], Fe_2O_3 or CuO particles or rods [23,24], or even diatomaceous earth [1], and employing various assembly techniques for tuning the contact area between the fuel and oxidizer [25–29].

As we all known, for a long period of time till now, Al, AP and NC are the commonly used fuel, oxidizer and energetic binder, respectively [19–24]. It will be ideal if we can create the

* Corresponding author.
E-mail address: mrz@umd.edu (M.R. Zachariah).

http://dx.doi.org/10.1016/j.combustflame.2017.02.036
0010-2180/

homogenous fuel/oxidizer/binder composites particles in one step. In this present paper, we employed an electrospray assembly technique to create visibly dense and homogeneously mixed submicron particles comprised of oxidizer-AP and binder-NC, and Al-NP's. The produced particles show rapid ignition, distinctly low ignition temperatures and high reactivity. Spectroscopic temperature measurements were performed on Al/AP/NC composites as well as Al/AP composite without NC. The potential ignition mechanism of the composites is also investigated.

2. Experimental

Materials: Aluminum nanoparticles (Al NPs, from Novacentrix Inc.) have an average diameter of ~80 nm with a ~2–5 nm oxide shell resulting in a ~81 wt% active Al content. The oxide shell thickness and active Al content were confirmed using transmission electron microscopy (TEM) and thermogravimetric analysis (TGA), respectively [30]. Ammonium perchlorate (AP, ~170 μm, 99.8 wt%, as shown in Fig. S1) and Collodion solution (4–8 wt. % in ethanol/diethyl ether) were purchased from Sigma-Aldrich Corp. All the materials were used as received. An acetone (99.8%) and methanol (99.8%) mixture (volume ratio: 1:5) was used to dissolve the AP. And a diethyl ether (99.8%)/Ethanol (99.8%) mixture (volume ratio: 1:3) was employed to dilute the collodion.

Precursor Preparation Procedure: The diluted collodion solution was mixed into the AP solution and was vigorously stirred for 1 h. Al NPs were gently added into the mixture followed by an hour of sonication. The stoichiometric ratio of Al/AP (equivalence ratio is 1.0) was calculated based on fully reaction between Al and AP with 81 wt% of active Al. NC was not taken into consideration when calculating the equivalence ratio. In a typical experiment (14 wt% NC, Al/AP equivalence ratio = 1.19), 157.2 mg AP was dissolved in the mixture of 0.5 mL acetone and 2.5 mL methanol to form the AP solution, and a mixture of 0.24 mL ethanol and 0.08 mL ether was added into 0.7 mL collodion solution. After mixing, 88.4 mg Al NPs were added into the final mixture. The as prepared suspension was sonicated for an hour and then magnetically stirred for 24 h. The process of preparing precursors for Al/AP without NC is exactly the same as above.

Electrospray Procedure: In this study we used a previously described electrospray process [31,32] to generate the composites. Electrospray is commonly used as a droplet cloud formation technique which advantages the balance between electric force and surface tension to produce uniform droplets. Following evaporation of the solvent in the droplets, uniform dry powders are obtained. In a typical electrospray experiment, the precursor prepared beforehand was loaded in a syringe and drove by a syringe pump. The feed rate was nominally 0.2 mL/h (0.5 and 1.0 mL/h were also employed, as labeled) through a 0.20 mm inner I.D. needle. An aluminum foil (24 cm × 24 cm) was served as the receiving substrate. The voltage applied between the needle and substrate was 18 kV at a distance of 2.5 cm. Due to the unstable suspension formed in the samples without NC, magnetic stirring was used to avoid any sedimentation of Al NPs. The described electrospray process was also employed with the same condition when creating AP, NC, and AP/NC particles.

Conventional physically mixed samples: The precursor for physically mixed sample is exactly the same as the electrospray case. In a typical experiment (14 wt% NC), 166.8 mg AP was dissolved in the mixture of 0.5 mL acetone and 2.5 mL methanol to form the AP solution, and a mixture of 0.24 mL ethanol and 0.08 mL ether was added into 0.7 mL collodion solution. After mixing, 78.8 mg Al NPs were added into the final mixture. The as prepared suspension was sonicated for an hour and then magnetically stirred for 24 h. The prepared precursor solution was then placed into a fume hood for 24 h to completely remove the solvent and then the remaining powder was gently broken into fine powder by a spatulas. The SEM image of the final Al/AP/NC particles made by physically mixed was shown in Fig. S8.

SEM, EDS, XRD and TG/DSC: A Hitachi Su-70 scanning electron microscope (SEM) with attached Energy-dispersive X-ray spectroscopy (EDS) was employed to analyze particle morphology and elemental composition, respectively. The composites were deposited onto a piece of aluminum foil during electrospray which was subsequently attached onto the SEM stage using carbon tape. A thin layer of Au (~3–5 nm) was deposited on the surface of the stage to increase the conductivity before testing. A Bruker D8, with Cu K radiation, X-ray diffractometer (XRD) was used to determine the crystallization state. Thermogravimetric/differential scanning calorimetry (TG/DSC) results were obtained with a TA Instruments Q600 at a rate of 5 °C/min up to a maximum temperature of 500 °C in an argon atmosphere.

Combustion cell characterization: The reactivity of the composites was evaluated in a constant volume (~13 cm^3) combustion cell, from which the pressure and optical emission histories can be simultaneously obtained. The details of combustion cell experiment can be found in our previous studies [33,34]. The pressurization rate was calculated from the initial slope of the pressure rise and the burn time was calculated from the full-width half-maximum of the optical emission history. Samples of 25 mg was tested three times and the average values were reported. The impulse was calculated from integral area under the time-resolved-pressure curve, which depends on overpressure and duration time.

T-jump ignition and time-resolved mass spectrometry: The details of the T-Jump ignition and time-resolved mass spectrometer system used in this study can be found in refs [34–36]. Typically, a ~10 mm long platinum filament (~76 μm in diameter) coated with the composite (~4 mm long) was resistively heated to ~1600 K (heating rate of $\sim 4 \times 10^5$ K s^{-1}) in 1 atm of Argon. The ignition and subsequent combustion of the composite was monitored using a high-speed camera (14.9 μs per frame with 256 × 256 pixels, Phantom V12.1). The time-resolved temperature profile of the wire was calculated from the temporal wire resistance recorded during the heating process and the ignition temperature was subsequently calculated by correlating the observed ignition timestamp from the high-speed video with the wire temperature profile. Time-resolved mass spectroscopy was also used for characterizing the species released during the fast heating. The ignition time is obtained from the time period between the wire triggering and the first light emission showing up.

Flame temperature measurement and adiabatic flame temperature calculation: The aforementioned T-Jump experiment was used for igniting the composite. The emission from the combustion event was collected by an optical fiber and sent to a 0.5 m spectrometer (Acton SP500i), which dispersed the light with a 150 g/mm grating. The spectrum was recorded by a 32 channel PMT (Hamamatsu) interfaced with a high-speed data acquisitions system (Vertilon IQSP 580). Time resolved spectra, in the 500–800 nm band, was sampled at 10 kHz and subsequently fit to Planck's law with grey body approximation to get time-resolved temperature [37]. The adiabatic flame temperature was calculated using the Cheetah 6.0 equilibrium code at a constant pressure with the alumina shell taken into account.

3. Results and discussion

3.1. Assembly and encapsulation of Al NPs within AP/NC matrix

Figure 1 shows SEM images and EDS mapping results of the formed Al/AP/NC composites. As Fig. 1a shows, multiple Al NPs are encapsulated in a transparent (to e-beam) matrix, which is a mixture of AP and NC. As Fig. S1 (supporting information) shows,

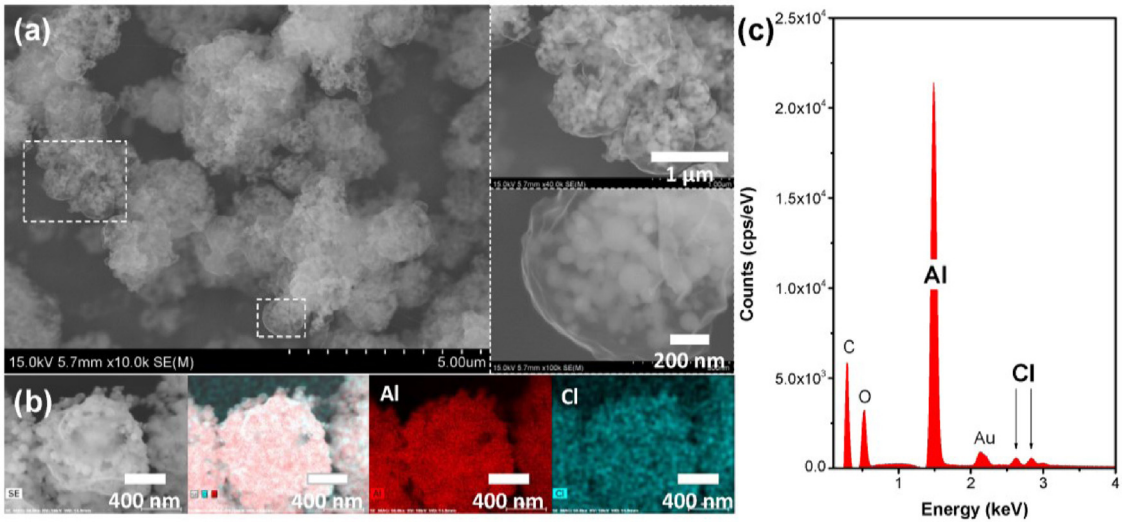

Fig. 1. Typical Low (a) and high (inserts of a) resolution SEM images, EDS mapping images of a single particle (b) and elemental result (c) of Al/AP/NC composites (14 wt% NC, Al/AP is in stoichiometric ratio). Note: the Au shows up because of the pre-process of gold coating. Feed rate: 1 mL/h.

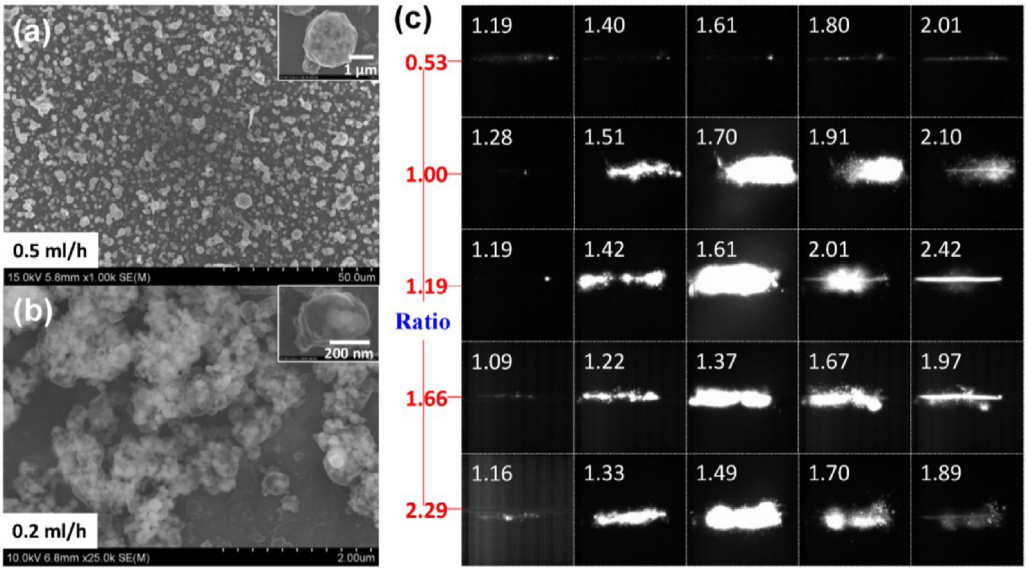

Fig. 2. The particles size can be tuned by applying different feed rates as 0.5 mL/h (a) and 0.2 mL/h (b) (14 wt% NC, Al/AP is in stoichiometric ratio). The combustion snapshots (c) of Al/AP/NC composites with different Al/AP equivalence ratios are shown. Note: the labeled in the snapshots are time after triggering.

both of NC and AP particles made by electrospray are transparent. However, the surface of the clear matrix melted and cracked slightly when exposed to the electron beam in the SEM. As a result, the particles shown in Fig. 1b and Fig. S1 are shrunk and not as transparent as particles that have not been exposed to the electron beam for such a long time (~10 minutes). The surface of AP crystals show a similar morphological change upon heating [38,39] supporting the claim that these changes are due to interactions with the electron beam. The EDS mapping results shown in Fig. 1b and c indicate that the Al NPs were well dispersed in the AP/NC matrix and the XRD results in Fig. S2 reveals that the AP is crystalline in the composites.

The size of the composites in Fig. 1a is in the range of 1–4 micron. And the size distribution can be easily tuned by the feed rate used during electrospray processing [17]. As Fig. 2a and b shows, the Al/AP/NC composites made with a feed rate of 0.5 mL/h and 0.2 mL/h have an average size of ~1.2 μm and ~0.5 μm, respectively. Composites with varying Al/AP ratios were also produced by electrospray using the same feed rate of 0.2 mL/h. The SEM images of these composites are shown in Fig. S3 and the size of these composites is also about ~0.5 μm. There is an observable increase in the packing density of Al NPs with increasing Al content in the composites.

All of the above Al/AP/NC composites were ignited on a rapidly-heated wire in 1 atm of argon, for which high speed video, and ignition temperatures, were obtained. It was found that the conventional physical mixed Al/AP/NC composites (Fig. S8) could not be ignited on the wire. That is because of the large crystals of AP and agglomerations of Al NPs result in substantial detachment between the gas phase combustion (AP/NC deflagration) and solid phase combustion (Al combustion). The slightly fuel-rich (1.19 equivalence ratio) Al/AP/NC composites visibly showed the most violent reaction, as Fig. 2c shows. The ignition temperature of the Al/AP/NC sample in Fig. 1 (size: ~1–4 μm) was ~980 K and the sample in Fig. 2a (size: ~1.2 μm) is ~890 K. Both have ignition temperatures around the melting point of Al (933 K), however, the sample in Fig. 2b (size: ~0.5 μm) could be ignited as low as 700 K. Note that the composition of these particles are the same while

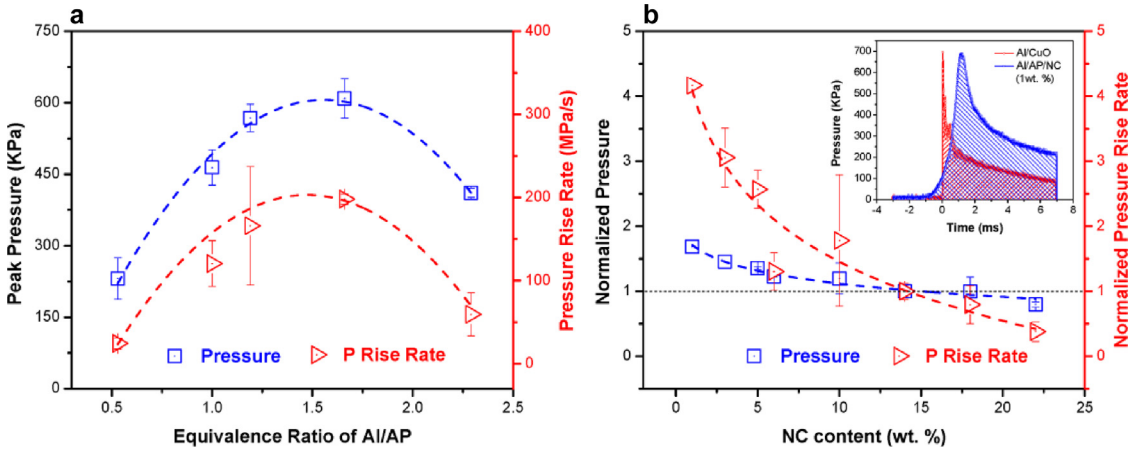

Fig. 3. Peak pressure, pressurization rate changes with the equivalence ratio of Al/AP (a, NC is 14 wt%) and the NC content (b, equivalent ratio: 1.19), respectively. Sample mass was fixed at 25.0 mg and three runs were conducted for each sample.

Table 1
Ignition time and temperature of different Al NPs containing composites.

Materials	Equivalence ratio	Ignition time (ms)	Ignition T (K) (±50 K)
Al/AP/NC composites (14 wt%, mean size: 0.5 μm)	0.53	1.2	710
	1.00	1.3	710
	1.19	1.2	730
	1.66	1.1	690
	2.29	1.1	720
Al/AP/NC mixture (14 wt%)	1.00	No ignition	n/a
Al/NC composites (10 wt%, mean size: 11.1 μm) [17]	1.00	3.3	n/a
Al/NC mixture (10 wt%) [17]	1.00	10.2	n/a
Al NPs (50 nm) [17]	n/a	17.1	n/a

only the size is different. Slow heat conduction in large particles might be one reason for their relative high ignition temperature. The ignition temperatures of all the Al/AP/NC composites (14 wt% NC) with a diameter of ~0.5 μm are approximately 700 K regardless of the Al/AP ratio (0.53-2.29) as Table 1 shows.

As Table 1 shows, previously synthesized Al/NC microparticles showed a short ignition delay time (0.3 ms, after 3 ms fast-heating) compared to Al NPs and Al/NC mixtures. As a consequence, propellants containing the Al/NC microparticles showed a burn rate increase of 35% [18]. We believe that the much shorter ignition delay time of Al/NC decreases the distance between burning Al NPs and burning surface of propellant (gas phase deflagration), thus providing better heat feedback to accelerate the combustion. In this study, as Table 1 shows, the Al/AP/NC composites were ignited rapidly (~1.2 ms). More importantly, the ignition temperatures of these composites are as low as ~700 K, which means that these Al containing composites might burn very close to the surface of propellant, thus potentially achieving high burn rate by taking full advantage of the high enthalpy of Al NPs and is being further investigated.

The reactivity of the Al/AP/NC composites was also evaluated using a confined volume combustion cell. From which we can obtain the peak pressure and pressurization rate of a chosen amount (25 mg) of material in a fixed volume (13 mL). The results for different Al/AP/NC composites with various Al/AP ratios were shown in Fig. 3a. Both the peak pressure and pressurization rate attains a maximum at an equivalence ratio of 1.66. Unlike the T-Jump test being conducted in argon, the combustion cell test was conducted in air, thus excess Al NPs will react with air, resulting in higher reactivity. The pressure and pressurization rate of Al/AP/NC composites with different NC contents were normalized to compare with the 14 wt% NC case. As Fig. 3b shows, both the pressure and pressurization rate drop dramatically with an increase of NC content because of NC's separation between the fuel (Al) and oxidizer (AP). However, it is important to note that the reactivity of the electrosprayed Al/AP without NC (as Fig. 4b shows) is so low that it is unable to trigger the data acquisition system (triggered from optical signal intensity). The reduction in reactivity (peak at 1 wt% NC) with increasing NC content of Al/AP/NC composites is different to what is observed for previous Al/CuO/NC mesoparticles [33], where reactivity peaked at ~5 wt% NC. In that study, NC not only acts as an energetic binder but also acts a gas generator to retard sintering of Al NPs. In the present study, AP itself is a good gas generator which can serve the same purpose as NC in retarding sintering. We note that the peak pressure of the Al/AP/NC composites is roughly the same as that of Al/CuO nanothermite, and the impulse is more than double (as the insert in Fig. 3b shows) because of enhanced gas release. Moreover, the Al/AP/NC composites (25 mg) with NC content ranging from 1 wt% to 22 wt% have impulse values as high as ~3.8 kN•s/m^2 (duration: −5 ms to 17.5 ms, as Table S1 shows), which indicates the potential of these composites as fuel source for propellants.

It is interesting to note that only 1 wt% of NC can bring a substantial increase in the reactivity of Al/AP composites. This can be explained by Fig. 4. For the Al/AP without NC (Fig. 4b), the fuel-Al NPs and the oxidizer-AP were not well mixed. The interfacial area between the two is largely reduced with the large aggregation of Al NPs and large crystallization of AP (>2 μm). The NC addition here is important because it not only acts like a stabilizer for the electrospray precursor to better mix the fuel and oxidizer in these composites (Fig. 4a, 1 wt% NC) and a binder for forming the submicron particles, but also ignites early and produces gas/heat to deflagrate AP and then finally contributes to ignite Al at low temperature (related video is in supporting material). As discussed before the micron size composite which has been demonstrated to burn faster in our prior studies [17,33], has been speculated to do so by both preventing sintering, but also by retarding heat loss to the surroundings thereby promoting combustion. The smaller sized AP has a lower decomposition temperature [19] which also with the above mentioned effects contribute to the high reactivity of Al/AP/NC composites. One important piece of forensic evidence is that the burning residues of Al/AP/NC composites are significantly smaller than those of Al/AP, revealing a more complete combustion of Al NPs and less sintering during combustion [40].

Flame temperature is a key parameter in parameters as heat feedback to the propellant surface significantly impacts burn rate. Figure 5a shows the temporal temperature profile of the Al/AP/NC

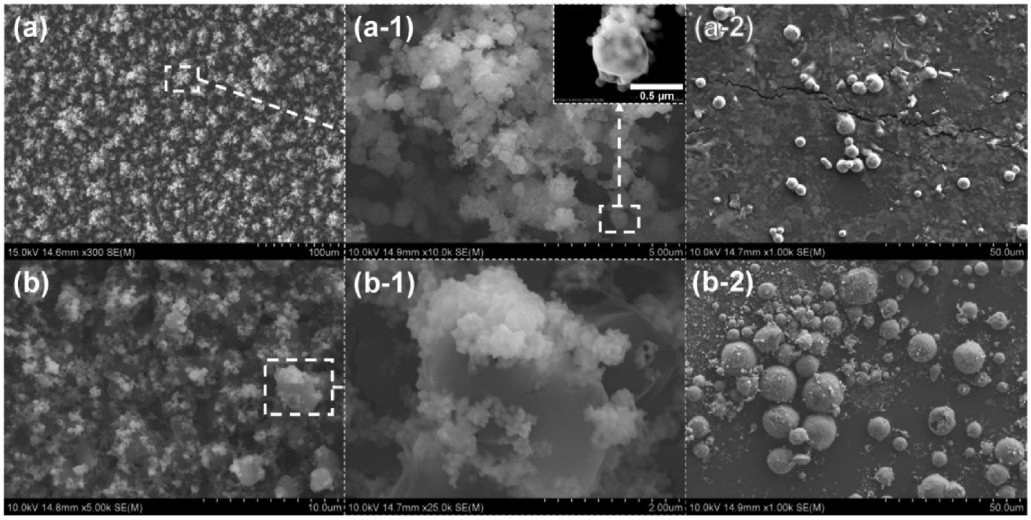

Fig. 4. The SEM images of Al/AP/NC composites (a and a-1, 1 wt% NC) and Al/AP composites (b and b-1, no NC) formed by electrospray. Both are in stoichiometric ratio. Al/AP/NC submicron particles (a-1 and the insert, 0.5 μm) aggregate into micron particles (a and a-1, 5-20 μm); Al NPs aggregate into submicron particles (b-1, ~0.5 μm) attached with micron AP crystals (b and b-1, 1-3 μm); the SEM images are the collected combustion residues from Al/AP/NC (a-2) and Al/AP (b-2), respectively.

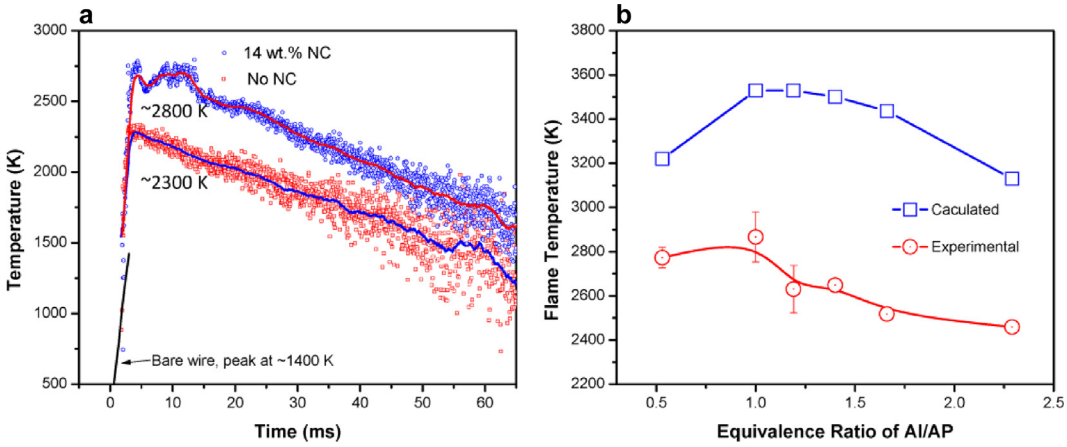

Fig. 5. The temperature-time history of bare wire (black line, obtained in T-Jump setup) and the flame temperature-time history (obtained in FT acquisition setup) of Al/AP (red square marks and blue line) and Al/AP/NC (blue round marks and red line, 14 wt% NC) composites (a, equivalence ratio is 1.0). The experimental flame temperature and calculated (constant pressure, by cheetah, H and H_2 are excluded in the products) adiabatic flame temperature results of Al/AP/NC with different Al/AP ratio (b, 14 wt% NC). (For interpretation of the references to color in this figure legend, the reader is referred to the web version of this article).

composite (14 wt% NC) and the Al/AP composite (no NC, see Fig. 4b). The peak flame temperature of the Al/AP/NC is ~500 K higher than that of the Al/AP, which peaks at ~2800 K within 4 ms. For comparison, the bare wire temperature ramps to ~1400 K in 3 ms. The flame temperatures of the Al/AP/NC composites with different Al/AP ratios were also measured, and the corresponding adiabatic flame temperatures calculated using the Cheetah software, are shown in Fig. 5b. Both of the calculated and experimental flame temperatures peak at the stoichiometric ratio of Al/AP, but in all cases the experimental measurements are several hundred degrees cooler than equilibrium calculation.

We now explore why the ignition temperatures of Al/AP/NC composites tabulated in Table 1 are so low. We conducted slow and fast heating experiments using TG/DSC and T-Jump MS, respectively. It is well known that AP decomposition can be divided into a low temperature stage (LTS) and a high temperature stage (HTS) (as Fig. 6 shows). In the LTS, AP decomposes to NH_3 and $HClO_4$ via proton transfer on the surface and defects of AP crystals, which also serve to slow down further decomposition until higher temperatures [19,38,41]. The thermal behavior of commercial AP (~170 μm), electrosprayed AP (~1 μm), commercial NC (dry film), electrosprayed AP/NC (~0.5 μm) and electrosprayed Al/AP/NC (~0.5 μm) composites are shown in Fig. 6. As Fig. 6a shows, commercial AP crystals (~170 μm) show an endotherm (243 °C) that corresponds to the transition from orthorhombic to a cubic phase. Further heating gives an exotherm (286 °C), followed by an endotherm (405 °C). However, the endotherm (405 °C) peak disappears when heating commercial AP in a pan with a pierced lid, while an exotherm occurs at ~433 °C. It has been suggested that the particular nature of the thermogram depends on the competition between sublimation (endothermic) and thermal decomposition (exothermic) [42,43,44].

For the electrospray AP the endothermic peak near 243 °C still remains, but seems to be overwritten by an exothermic peak at 240 °C, which is probably induced by an early partial decomposition of AP. From Fig. 6b, we can see that electrosprayed AP starts to decompose at 224 °C, nearly 50 °C earlier than commercial AP. The most significant change of electrosprayed AP compared to commercial AP is the disappearance of the endothermic peak (~405 °C) caused by sublimation. The major decomposition exothermic peak of electrosprayed AP shows up at ~329 °C, which is ~100 °C earlier compared to commercial AP (further confirmed by TGA in Fig. 6b). We contribute this change partially to the much faster heat conduction among electrosprayed AP particles (~1 μm) compared to

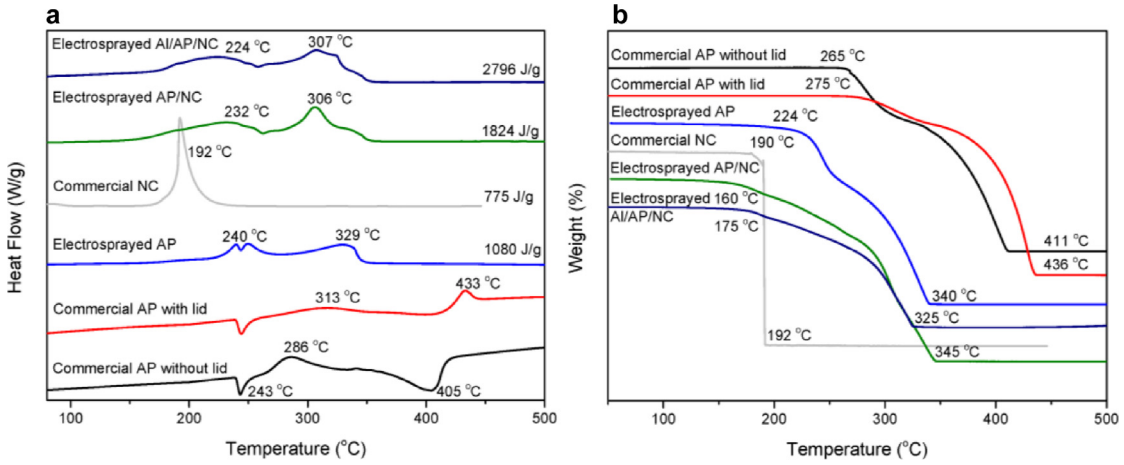

Fig. 6. Heat flow results (a) weight-loss curves (b, up is exothermal) from TG/DSC test (5 K/min) of commercial AP (with and without lid), NC, electrosprayed AP, AP/NC, and Al/AP/NC composites.

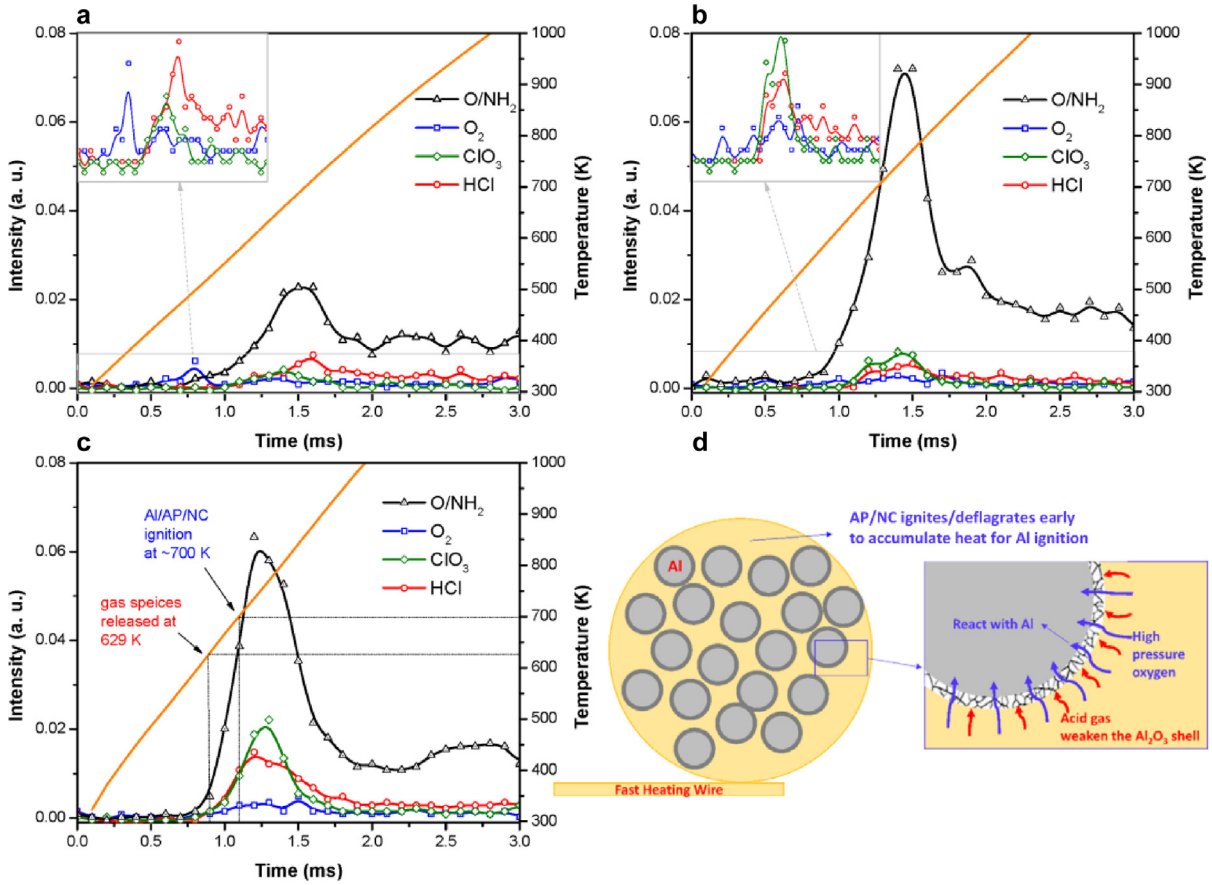

Fig. 7. Time-resolved released species intensities from AP (a), AP/NC (b) and Al/AP/NC (c) in T-Jump MS, and the possible ignition process of Al/AP/NC composites (d).

commercial materials (~170 μm), but perhaps more importantly to the recrystallization of AP with more defects [39]. As Fig. 6a and b shows, NC has completely decomposed by ~190 °C. With the addition of NC, the electrosprayed AP/NC has a smaller size of ~0.5 μm. The endothermic peak of phase transition almost disappear owing to the thermal decomposition of NC and early thermal decomposition of AP. Moreover, the major thermal decomposition of AP/NC peaks at ~306 °C, which is almost 130 °C earlier compared to the commercial AP.

The TG/DSC curves between Al/AP/NC and AP/NC composites show no difference except the decomposition heat. The decomposition heat (~2796 J/g) for Al/AP/NC is >50% and 160 % larger when compared to electrosprayed AP/NC (~1824 J/g) and AP (~1080 J/g), respectively. It is possible however that the alumina cap on the Al NPs might catalyze the decomposition but doesn't itself participate because of the temperature is too low for Al oxidation reaction.

The ignition temperatures of the Al/AP/NC composites with varying NC content were also measured. The SEM images of the Al/AP/NC composites with different NC content can be found in Fig. S4. The Al/AP composites without NC (produced by electrospray) had an ignition temperature of ~1400 K (Fig. S7), which may be due to the large AP crystals (>2 μm), large aggregation

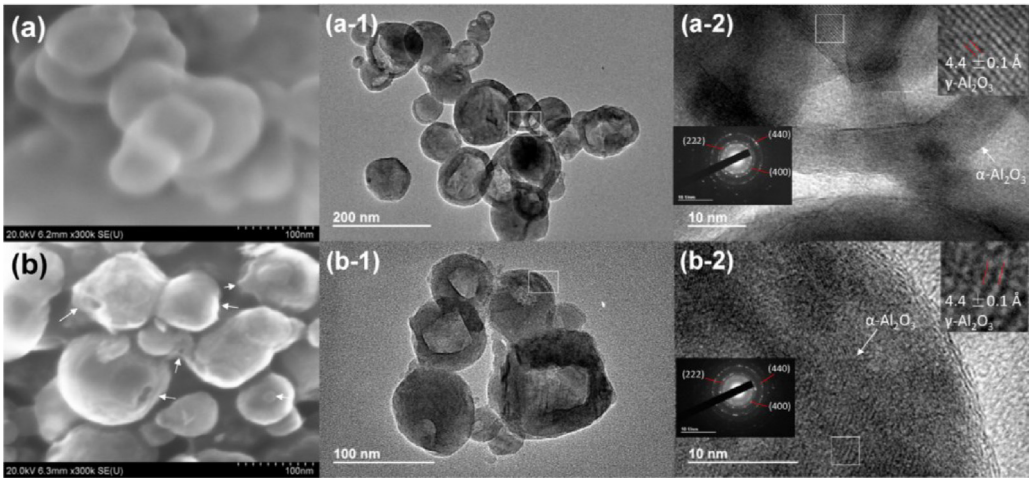

Fig. 8. High resolution SEM (a and b)/TEM (a-1, a-2, b-1 and b-2) images and diffraction patterns (left insert images of a-2 and b-2) of final products from TG/DSC experiments of (a) Al NPs and (b) Al/AP/NC composites (5 °C/min, to 1000 °C in argon).

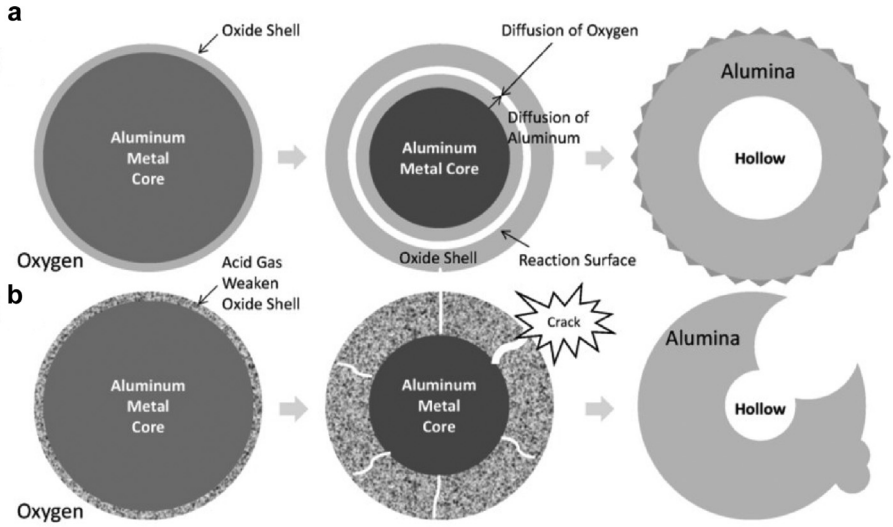

Fig. 9. Schematic of the two different mass transfer mechanism of Al NPs and Al/AP/NC upon heating.

of Al NPs and poor mixing of Al with AP (Fig. 4b and 4b-1). After adding a small percentage of NC (from 1 wt% to 10 wt%), the ignition temperatures of the composites drop dramatically to the melting point of Al NPs (~933 K), which traditionally is the lower limit for Al-based thermite ignition. With the NC content further increases to 14 wt% and 22 wt%, the ignition of the composites occurs at ~730 K, which is ~200 K lower than Al's melting point.

We now turn our attention to fast heating as shown in Fig. 7a–c. AP decomposition (Fig. 7a) shows oxygen evolution ~500 K, which is corresponding to the low temperature stage (LTS) decomposition of AP. The major decomposition products, HCl and ClO_3 peak at ~680 K, which corresponds to the high temperature stage (HTS) of AP decomposition. From Fig. S5a, we can see hydrocarbons, oxycarbide and oxynitride etc. early in the process, and is indicative of NC decomposition at low temperature. With the addition of NC, as Fig. 7b shows, the AP/NC shows reduced O_2 owing to its participation in NC's decomposition. However, we also observe much higher O/NH_2, ClO_3 peaks owing to the promoted AP decomposition attributed by NC. With the addition of Al NP's we observe in Fig. 7c, much higher ClO_3 and HCl. The major degradation products such as ClO_3, ClO_2, ClO, HCl and O_2 (Fig. S5) from AP appears at ~630 K and peak around ~750 K (Fig. 7a and Fig. S5b) while the ignition temperature for the Al/AP/NC composites was measured as ~700 K, which is further confirmed by the spectra in Fig. S5d, where AlO and Al_2O appear.

Based on these results we conjecture as to why the electrosprayed Al/AP/NC composites can be ignited at such low temperatures. The most likely explanation is that the high dispersion of AP/Al/NC system as generated by the electrosprayed mesoparticles enables for a better exposure of the alumina shell in Al NP's to the AP decomposition products which are highly corrosive (acid gases) [45]. Evidence for interaction with the alumina shell comes from our mass spectrometry results showing $AlCl_2$ species (Fig. S5d), which appear at the same time as AlO and Al_2O.

To further corroborated this mechanism we conducted slow heating (5 °C/min) studies in argon to 1000 °C of Al NPs and Al/AP/NC composites. The resultant solid products were inspected by SEM. For Al NPs case, as Fig. 8a shows, the resultant particles are hollow indicating that molten aluminum has leaked through the alumina shell (Fig. S9a), but that the shell has maintained its integrity. The shell thickness is around 6–16 nm, which varies with the size of particles. The shells mainly consists of γ-Al_2O_3 (PDF #10-0425), which is confirmed by electron diffraction patterns and the lattice parameters. These results are consistent with prior work on heating of Al NPs above its melting point [46–52]. In contrast for Al/AP/NC case, as Fig. 8b and 8b-1 shows, almost every

particle has a hole(s) in the surface. And while the particles also have a hollow structure their shell seems to be thicker as compared to the case of Al NPs. The electron diffraction patterns and lattice size in Fig. 8b-2 also confirm the material is primarily γ-Al_2O_3. This results is corroborating evidence for the degradation of the alumina shell by AP decomposition products.

Generally, the oxidization process of Al NPs can be roughly divided into two main stages by the Al melting point. Below the Al melting point, the diffusion of oxygen or aluminum species through the oxide layer is slow, but will considerably increase after melting, driven by internal pressure gradients and built-in electric fields among the particles [46–47,53]. As a consequence, of the higher diffusivity of Al ions, the final particles are hollow with a much thicker shell [49] (Fig. 9a and Fig. S9a). With the addition of AP which releases acid gases as low as ~630 K reaction with the alumina shell commences, significantly weakening it and presumably leading to cracks and holes which expose unreacted aluminum to the oxidizer (Fig. 9b and Fig. S9b). The formation of an encapsulated structure enhances the contact between AP and Al NP's, which promote the acid gas attack on the alumina shell, and thus lowering ignition temperature.

4. Conclusion

In summary, we use electrospray techniques to fabricate Al/AP/NC composites with well-dispersed Al NPs encapsulated within an AP/NC matrix. The ignition temperature, reactivity and flame temperature of different Al/AP composites with different NC content and Al/AP ratio were characterized. The composites with 14 wt% NC (~0.5 μm) show ignition temperatures ~200 K lower than Al melting point, possesses a high gas generator ability, as well as high flame temperature. The possible mechanism of the early ignition of the composites was also proposed and investigated. We attribute the low ignition temperature to the release of acid gas from AP which can etch the alumina shell. This paper might provide a potential approach for making high-speed burning propellant in one step.

Associated content

Supporting Information is free to be downloaded at: http://www.sciencedirect.com/science/journal/001,02180.

Acknowledgments

This work was supported by the Defense Threat Reduction Agency and the Army Research Office. We acknowledge the support of the Maryland Nanocenter and its NispLab. The NispLab is supported in part by the NSF as a MRSEC Shared Experimental Facility.

Supplementary materials

Supplementary material associated with this article can be found, in the online version, at doi:10.1016/j.combustflame.2017.02.036.

References

[1] S. Shioya, M. Kohga, T. Naya, Burning characteristics of ammonium perchlorate-based composite propellant supplemented with diatomaceous earth, Combust. Flame 2 (2014) 620–630.
[2] V.A. Arkhipov, A.G. Korotkikh, The influence of aluminum powder dispersity on composite solid propellants ignitability by laser radiation, Combust. Flame 1 (2012) 409–415.
[3] S. Sadeghipour, J. Ghaderian, M.A. Wahid, Advances in aluminum powder usage as an energetic material and applications for rocket propellant, AIP Conf. Proc. 1440 (2012) 100–108.
[4] A. Dokhan, E.W. Price, J.M. Seitzman, R.K. Sigman, The effects of bimodal aluminum with ultrafine aluminum on the burning rates of solid propellants, Proc. Combust. Inst 2 (2002) 2939–2946.
[5] E.L. Dreizin, Metal-based reactive nanomaterials, Prog. Energy Combust. Sci. 2 (2009) 141–167.
[6] V.A. Ermakov, A.A. Razdobreev, A.I. Skorik, V.V. Pozdeev, S.S. Smolyakov, Temperature of aluminum particles at the time of ignition and combustion, Combust. Explos. Shock Waves 2 (1982) 256–257.
[7] R. Friedman, A. Maček, Ignition and combustion of aluminium particles in hot ambient gases, Combust. Flame 6 (1962) 9–19.
[8] E.W. Price, R.K. Sigman, Combustion of aluminized solid propellants, Solid propellant chemistry, combustion and motor interior ballistics, progress in astronautics and aeronautics, AIAA, vol. 185, Reston, VA (2000), pp. 663–687.
[9] C. Zanotti, A. Volpi, M. Bianchessi, L DeLuca, Measuring thermodynamic properties of burning propellants, Nonsteady burning and combustion stability of solid propellants, progress in astronautics and aeronautics, AIAA, vol. 143, Washington, DC (1992), pp. 145–196.
[10] T. Bazyn, H. Krier, N. Glumac, Combustion of nanoaluminum at elevated pressure and temperature behind reflected shock waves, Combust. Flame 4 (2006) 703–713.
[11] R.A. Yetter, G.A. Risha, S.F. Son, Metal particle combustion and nanotechnology, Proc. Combust. Inst 2 (2009) 1819–1838.
[12] L.T. DeLuca, L. Galfetti, G. Colombo, F. Maggi, A. Bandera, V.A. Babuk, V.P. Sinditskii, Microstructure effects in aluminized solid rocket propellants, J. Propul. Power 4 (2010) 724–732.
[13] L. Galfetti, L.T. De Luca, F. Severini, L. Meda, G. Marra, M. Marchetti, M. Regi, S. Bellucci, Nanoparticles for solid rocket propulsion, J. Phys.: Condens. Matter 33 (2006) S1991.
[14] L. Galfetti, L.T. DeLuca, F. Severini, G. Colombo, L. Meda, G. Marra, Pre and post-burning analysis of nano-aluminized solid rocket propellants, Aerosp. Sci. Technol. 1 (2007) 26–32.
[15] J. Zhi, L. Shu-Fen, Z. Feng-Qi, L. Zi-Ru, Y. Cui-Mei, L. Yang, L. Shang-Wen, Research on the combustion properties of propellants with low content of nano metal powders, Propellants Explos. Pyrotech. 2 (2006) 139–147.
[16] E.W. Price, Combustion of metalized propellants, Fundamentals of solid propellant combustion, progress in astronautics and aeronautics, AIAA, vol. 90, New York, NY (1984), pp. 479–513.
[17] H. Wang, G. Jian, S. Yan, J.B. DeLisio, C. Huang, M.R. Zachariah, Electrospray formation of gelled nano-aluminum microspheres with superior reactivity, ACS Appl. Mater. Interfaces 15 (2013) 6797–6801.
[18] G. Young, H. Wang, M.R. Zachariah, Application of nano-aluminum/nitrocellulose mesoparticles in composite solid rocket propellants, Propellants Explos. Pyrotech. 40 (2015) 413–418.
[19] S. Isert, T.D. Hedman, R.P. Lucht, S.F. Son, Oxidizer coarse-to-fine ratio effect on microscale flame structure in a bimodal composite propellant, Combust. Flame 163 (2016) 406–413.
[20] S. Jain, S.Nandagopal Mehilal, P.P. Singh, K.K. Radhakrishnan, B. Bhattacharya, Size and shape of ammonium perchlorate and their influence on properties of composite propellant, Def. Sci. J. 59 (2009) 294–299.
[21] A.N. Ali, S.F. Son, M.A. Hiskey, D.L. Naud, Novel high nitrogen propellant use in solid fuel micropropulsion, J. Propul. Power 1 (2004) 120–126.
[22] S. Isert, C.D. Lane, I.E. Gunduz, S.F. Son, Tailoring burning rates using reactive wires in composite solid rocket propellants, Proc. Combust. Inst 2 (2016) 2283–2290.
[23] A.A. Vargeese, A kinetic investigation on the mechanism and activity of copper oxide nanorods on the thermal decomposition of propellants, Combust. Flame 165 (2016) 354–360.
[24] T.D. Hedman, D.A. Reese, K.Y. Cho, L.J. Groven, R.P. Lucht, S.F. Son, An experimental study of the effects of catalysts on an ammonium perchlorate based composite propellant using 5 kHz PLIF, Combust. Flame 4 (2012) 1748–1758.
[25] S. Subramanium, S. Hasan, S. Bhattacharya, Y. Gao, S. Apperson, M. Hossain, R. Shende, S. Gangopadhyay, P. Redner, D. Kapoor, Self-assembled ordered energetic composites of CuO nanorods and nanowells and Al nanoparticles with high burn rates, Mater. Res. Soc. Symp. Proc. 896 (2005) 9–14.
[26] J.Y. Malchi, T.J. Foley, R.A. Yetter, Electrostatically self-assembled nanocomposite reactive microspheres, ACS Appl. Mater. Interfaces 11 (2009) 2420–2423.
[27] J.L. Cheng, H.H. Hng, H.Y. Ng, P.C. Soon, Y.W. Lee, Synthesis and characterization of self-assembled nanoenergetic Al-Fe_2O_3 thermite system, J. Phys. Chem. Solids 2 (2010) 90–94.
[28] C. Rossi, S. Orieux, B. Larangot, T. Do Conto, D. Estève, Design, fabrication and modeling of solid propellant microrocket-application to micropropulsion, Sens. Actuators, A 1 (2002) 125–133.
[29] C. Rossi, K. Zhang, D. Esteve, P. Alphonse, P. Tailhades, C. Vahlas, Nanoenergetic materials for MEMS: a review, J. Microelectromech. Syst. 4 (2007) 919–931.
[30] P.M. Guerieri, S. DeCarlo, B. Eichhorn, T. Connell, R.A. Yetter, X. Tang, Z. Hicks, K.H. Bowen, M.R. Zachariah, Molecular aluminum additive for burn enhancement of hydrocarbon fuels, J. Phys. Chem. A 45 (2015) 11084–11093.
[31] H. Wang, J.B. DeLisio, G. Jian, W. Zhou, M.R. Zachariah, Electrospray formation and combustion characteristics of iodine-containing Al/CuO nanothermite microparticles, Combust. Flame 7 (2015) 2823–2829.
[32] H. Wang, G. Jian, W. Zhou, J.B. DeLisio, V.T. Lee, M.R. Zachariah, Metal iodate-based energetic composites and their combustion and biocidal performance, ACS Appl. Mater. Interfaces 31 (2015) 17363–17370.
[33] H. Wang, G. Jian, G.C. Egan, M.R. Zachariah, Assembly and reactive properties of Al/CuO based nanothermite microparticles, Combust. Flame 8 (2014) 2203–2208.

[34] G. Jian, J. Feng, R.J. Jacob, G.C. Egan, M.R. Zachariah, Super-reactive nanoenergetic gas generators based on periodate salts, Angew. Chem. Int. Ed 37 (2013) 9743–9746.
[35] L. Zhou, N. Piekiel, S. Chowdhury, M.R. Zachariah, T-Jump/time-of-flight mass spectrometry for time-resolved analysis of energetic materials, Rapid Commun. Mass Spectrom. 1 (2009) 194–202.
[36] L. Zhou, N. Piekiel, S. Chowdhury, M.R. Zachariah, Time-resolved mass spectrometry of the exothermic reaction between nanoaluminum and metal oxides: the role of oxygen release, J. Phys. Chem. C 33 (2010) 14269–14275.
[37] D. Ng, G. Fralick, Use of a multiwavelength pyrometer in several elevated temperature aerospace applications, Rev. Sci. Instrum 72 (2001) 1522–1530.
[38] N. Gurram, S.R. Chakravarthy, Experimental investigation of cellular instability in Ammonium Perchlorate (AP) and fine AP-binder mixtures, Proc. Combust. Inst. 2 (2015) 2455–2461.
[39] T.D. Hedman, M.L. Gross, On the thermal stability of partially decomposed ammonium perchlorate, Propellants Explos. Pyrotech. 2 (2016) 254–259.
[40] R.J. Jacob, B. Wei, M.R. Zachariah, Quantifying the enhanced combustion characteristics of electrospray assembled aluminum mesoparticles, Combust. Flame 167 (2016) 472–480.
[41] M. Plaud, S. Gallier, M. Morel, Simulations of heterogeneous propellant combustion: effect of particle orientation and shape, Proc. Combust. Inst. 2 (2015) 2447–2454.
[42] A.J. Lang, S. Vyazovkin, Effect of pressure and sample type on decomposition of ammonium perchlorate, Combust. Flame 145 (2006) 779–790.
[43] S. Vyazovkin, C.A. Wight, Kinetics of thermal decomposition of cubic ammonium perchlorate, Chem. Mater. 11 (1999) 3386–3393.
[44] H. Zhao, X. Zhu, Y. Shang, S. Chen, B. Li, Z. Bian, Ferrocene and [3] ferrocenophane-based β-diketonato copper (ii) and zinc (ii) complexes: synthesis, crystal structure, electrochemistry and catalytic effect on thermal decomposition of ammonium perchlorate, RSC Adv 6 (2016) 34476–34483.
[45] W.K. Lewis, B.A. Harruff, J.R. Gord, A.T. Rosenberger, T.M. Sexton, E.A. Guliants, C.E. Bunker, Chemical dynamics of aluminum nanoparticles in ammonium nitrate and ammonium perchlorate matrices: enhanced reactivity of organically capped aluminum, J. Phys. Chem. C 1 (2011) 70–77.
[46] A. Rai, D. Lee, K. Park, M.R. Zachariah, Importance of phase change of aluminum in oxidation of aluminum nanoparticles, J. Phys. Chem. B 39 (2004) 14793–14795.
[47] A. Rai, K. Park, L. Zhou, M.R. Zachariah, Understanding the mechanism of aluminium nanoparticle oxidation, Combust. Theor. Model. 5 (2006) 843–859.
[48] D.A. Firmansyah, K. Sullivan, K. Lee, Y.H. Kim, R. Zahaf, M.R. Zachariah, D. Lee, Microstructural behavior of the alumina shell and aluminum core before and after melting of aluminum nanoparticles, J. Phys. Chem. C 1 (2012) 404–411.
[49] M. Coulet, B. Rufino, P. Esposito, T. Neisius, O. Isnard, R. Denoyel, Oxidation mechanism of aluminum nanopowders., J. Phys. Chem. C 44 (2015) 25063–25070.
[50] C. Kong, D. Yu, S. Li, Q. Yao, Mechanism and modelling of aluminium nanoparticle oxidation coupled with crystallisation of amorphous Al_2O_3 shell, Combust. Theor. Model. 2 (2016) 296–312.
[51] A.B. Vorozhtsov, M. Lerner, N. Rodkevich, H. Nie, A. Abraham, M. Schoenitz, E.L. Dreizin, Oxidation of nano-sized aluminum powders, Thermochim. Acta 636 (2016) 48–56.
[52] M.A. Trunov, M. Schoenitz, E.L. Dreizin, Effect of polymorphic phase transformations in alumina layer on ignition of aluminium particles, Combust. Theor. Model. 4 (2006) 603–623.
[53] B.J. Henz, T. Hawa, M.R. Zachariah, On the role of built-in electric fields on the ignition of oxide coated nanoaluminum: ion mobility versus Fickian diffusion, J. Appl. Phys. 2 (2010) 024901.